

VU Research Portal

Erosion and diapirism: a comparative analysis of salt diapirism for different cases of erosion

Poliakov, A.; van Balen, R.T.; Podlachikov, Y.; Daudre, B.; Cloetingh, S.A.P.L.; Talbot, C.

published in

Tectonophysics

1993

document version

Publisher's PDF, also known as Version of record

[Link to publication in VU Research Portal](#)

citation for published version (APA)

Poliakov, A., van Balen, R. T., Podlachikov, Y., Daudre, B., Cloetingh, S. A. P. L., & Talbot, C. (1993). Erosion and diapirism: a comparative analysis of salt diapirism for different cases of erosion. *Tectonophysics*, 226, 199-216.

General rights

Copyright and moral rights for the publications made accessible in the public portal are retained by the authors and/or other copyright owners and it is a condition of accessing publications that users recognise and abide by the legal requirements associated with these rights.

- Users may download and print one copy of any publication from the public portal for the purpose of private study or research.
- You may not further distribute the material or use it for any profit-making activity or commercial gain
- You may freely distribute the URL identifying the publication in the public portal ?

Take down policy

If you believe that this document breaches copyright please contact us providing details, and we will remove access to the work immediately and investigate your claim.

E-mail address:

vuresearchportal.ub@vu.nl

Numerical analysis of how sedimentation and redistribution of surficial sediments affects salt diapirism

A.N.B. Poliakov ^{a,*} R. van Balen ^b, Yu. Podladchikov ^c, B. Daudre ^b, S. Cloetingh ^b
and C. Talbot ^a

^a Hans Ramberg Tectonic Laboratory, Institute of Earth Sciences, Uppsala University, Norbyvägen 18B, S-752 36 Uppsala, Sweden

^b Institute of Earth Sciences, Vrije Universiteit, 1081 HV Amsterdam, The Netherlands

^c Institute of Experimental Mineralogy, Russian Academy of Sciences, Chernogolovka, 142 432, Moscow District, Russia

(Received August 13, 1992; revised version accepted February 16, 1993)

ABSTRACT

Two-dimensional finite-element models are used to study how sedimentation and redistribution of sediments on the upper surface affects the development of subsurface salt diapirs. A rising diapir creates a bulge flanked by topographic lows in a generally accumulating sedimentary pile. We find that the rate at which this topography is flattened by erosion and redeposition controls the style of diapirism. This is because the redistribution of material from topographic highs to flanking lows is equivalent to changing the effective forces acting on the salt. Redistributing a potential topography modulates diapiric growth rate.

The main effects of including surficial sediment redistribution in numerical models of diapirism are: (1) diapirs grow 10–100 times faster; (2) diapirs may rise above their level of neutral buoyancy and extrude; (3) diapirs assume “finger” or “stock” like shapes rather than “mushroom” or balloon-on-string shapes; and (4) layers in the surrounding sediments remain nearly horizontal and only steepen sharply near the diapir. In effect, the rate of redistribution of surficial overburden strongly controls the mode of diapirism. Sediment redistribution (referred to as erosion for brevity) is modeled using a one dimensional diffusion equation. We show the results of two different erosion rates: infinitely slow (no erosion) and extremely fast (which redistributes surficial sediments but does not remove them from the system). We show that the shapes of model diapirs rising beneath surfaces subjected to rapid erosion simulate salt diapirs in the Gulf of Mexico. Columnar diapirs indicate rapid deposition on the shelf and plug-like diapirs slow sedimentation on the abyssal plane. Diapirs rising beneath surfaces with negligible erosion have the “mushroom” shapes interpreted for salt diapirs in central Iran.

Introduction

Seismic profiles and drilling demonstrate that salt diapirs have a wide variety of shapes (e.g., Jackson and Seni, 1984; Worral and Snelson, 1989; Nelson, 1991). These shapes reflect the many ways in which salt diapirs interacted with their overburden as they grow. Salt diapirs can actively pierce overburdens deposited before they start to build up, or they can passively pierce overburdens that are built down around them (Jackson and Talbot, 1991). The shapes of built up active diapirs have been the subject of many

earlier model studies. There have been far fewer studies of how the downbuilding of overburdens affect the shape of salt diapirs (e.g., Jackson et al., 1988). Here we study the dynamics of downbuilding overburdens around salt diapirs. We recognize that overburdens to natural diapirs can contain igneous and carbonate rocks, etc., but simplify our discussion here by treating all overburden as clastic sediments added to the top surface. We also refer all deformations to the bottom boundary and so that we write about even builddown diapirs as rising.

We use numerical models to explore how different rates of general sedimentation, together with local erosion and redeposition, affect the evolution of buoyant salt structures rising from depth. Our results allow deduction of information

* Present address: HLRZ, KFA- Jülich, Postfach 1913, 52425 Jülich, Germany.

about the history of a sedimentary basin from the shapes of its diapirs and their relations with the sediments that surround them.

Biot and Ode (1965) were the first to perform stability analyses for the initial stages of Rayleigh–Taylor instabilities where compacting clastic overburdens were eroded and resedimented on the upper surface. These workers showed that erosion and resedimentation of the surface bulge that develops over rising diapirs significantly accelerates the rise of the diapirs. The influence of this surficial redistribution increases in importance as the viscosity contrast between the salt and sediments increases, and as the salt–sediment interface nears the surface. Analytical models have been proposed for the growth rate of fully developed diapirs (Lerche and O'Brien, 1987) and the shape of extruding diapirs (Talbot and Jarvis, 1984). However, such analytical models constrain the shapes of diapirs and their relations with surrounding overburden only for particular stages. To understand the complete history of a diapir we need numerical or analog simulation of the whole diapiric process.

Different aspects of salt diapirism have been modeled numerically by many investigators (e.g., Woidt, 1978; Schmeling, 1987; Romer and Neugebauer, 1991; Zaleski and Julien, 1992; Van Keken et al., 1993). However, none of these models included the redistribution of surficial overburden over the upper surface which we will show here to be one of the crucial factors controlling the style of diapirism.

Jackson et al. (1988) and Talbot (1992) used analog models with viscous rheologies to explore how the shapes of diapirs relate to their history of loading by overburdens of different types. Analog modeling by Vendeville and Jackson (1992a,b) showed that faulting during thin-skinned horizontal extension of brittle overburdens can initiate diapirs that rise or fall. Erosion has been simulated in centrifuge modeling of diapirism by stopping the experiment and flattening the upper surface (H. Ramberg, pers. commun., 1992). However, such step-wise loading is a major drawback for studies of a smooth and continuous process like diapirism.

We present here the results of numerical mod-

els of diapir–sediment interaction that include compaction, sedimentation, erosion and redeposition. We simulate the growth of viscous diapirs in viscous overburdens using the numerical technique developed by Poliakov and Podladchikov (1992) which can solve problems with a stress-free upper boundary.

The overburden is treated here as a highly viscous Newtonian fluid because:

(1) Some natural overburdens exhibit ductile behavior (see for example seismic profiles in Jenyon (1986) and satellite pictures of the Great Kavir, Iran (see Fig. 1).

(2) As we shall show, the effects of erosion and sedimentation are likely to have a far stronger impact on diapirism than a more precise descriptions of their overburden rheology.

(3) Models with simple Newtonian overburdens closely resemble profiles of many natural diapirs.

(4) It is still very difficult to include viscous and brittle rheologies in the same numerical code for studies of the large strains inherent in diapirism [the authors are working in this direction (Daudre et al., 1992; Poliakov et al., 1992; Podladchikov et al., 1993)].

Sedimentation, erosion and redeposition are modeled using a one dimensional diffusion equation (Kenyon and Turcotte, 1985; Syvitski et al., 1988) with a constant transportation coefficient. Sediments are added via the source term and no sediments can escape from the box (i.e., there is zero flux for sediment across all boundaries but the top). We find that model diapirs that develop beneath surfaces with redistributed topographies *differ considerably* from models without such erosion and redeposition. This difference has a simple physical explanation. Consider an imaginary horizontal mean upper surface. A buoyantly rising diapir lifts and bulges the surface immediately above it. The topographic weight of this positive relief balances the buoyancy force and the vertical stress on the mean upper surface consequently equals zero. Erosion removes this local topography, unbalancing the vertical stress on the imaginary surface. This is equivalent to an additional force pulling the diapir upwards. At the same time, redeposition of the eroded material in

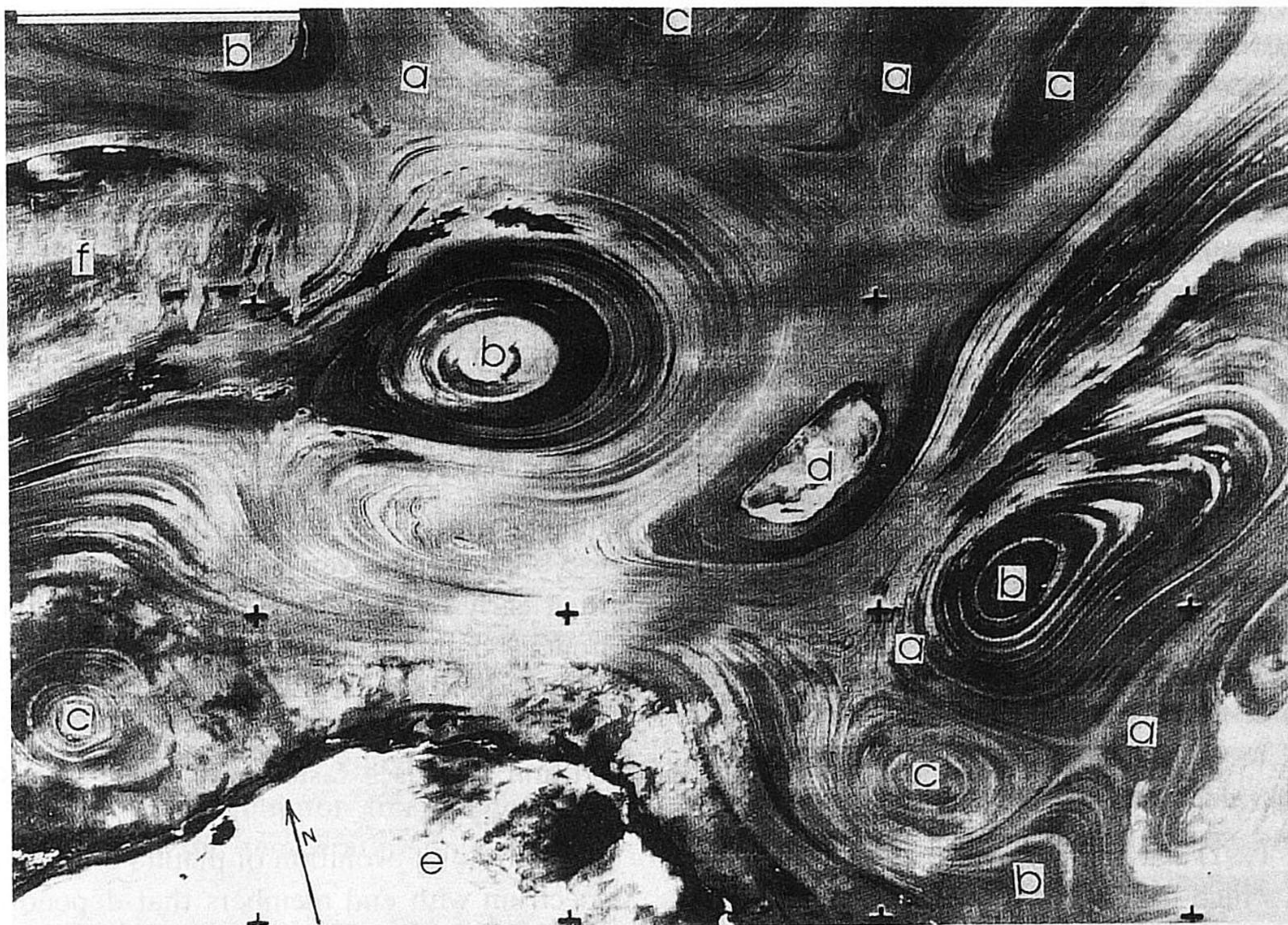


Fig. 1. Landsat image of Great Kavir pediment, showing an erosional section through two basins (b) and two domes (c) that developed in entirely ductile rocks (from Jackson et al., 1990).

adjacent topographic lows applies additional downward acting forces on the surface. The two sets of forces resulting from redistribution of the potential topography caused by a rising diapir combine to speed up the diapirism.

We show that surficial sediment redistribution plays a key role in salt diapirism. Including erosion and resedimentation in numerical analysis of diapirism has several major effects:

- (1) diapiric growth is accelerated;
- (2) diapir shapes change to “finger” or “stock-like”;
- (3) diapirs extrude onto the top surface;
- (4) layers in the overburden deform with different styles.

Such distinctive differences allow prediction of the type of diapirism from analysis of the surface processes or vice versa. Thus climatic conditions that imply negligible erosion also imply that subsurface diapirs are likely to have “mushroom” shapes. Conversely, diapirs that rise beneath surfaces subjected to rapid erosion and resedimenta-

tion are likely to have shapes like “fingers” or “plugs”.

Influence of erosion on diapiric dynamics

Typical boundary conditions for the simulation of tectonic processes are presented in Figure 2.

The most popular top boundary condition for previous numerical models of diapirs has been free-slip (Fig. 2a). This is because free-slip can easily be implemented for rectangular Eulerian meshes. The upper surface remains flat all the time, but the topography can be estimated a posteriori from the vertical stresses acting on it. A moving Lagrangian mesh is appropriate for studying the evolution of a free surface (i.e., a stress-free top boundary condition; Fig. 2b). In this approach the numerical mesh tracks the particle paths. Topographies for most geophysical problems are generally similar if they are followed using either free-surface and free-slip upper boundary conditions (Poliakov and Podlad-

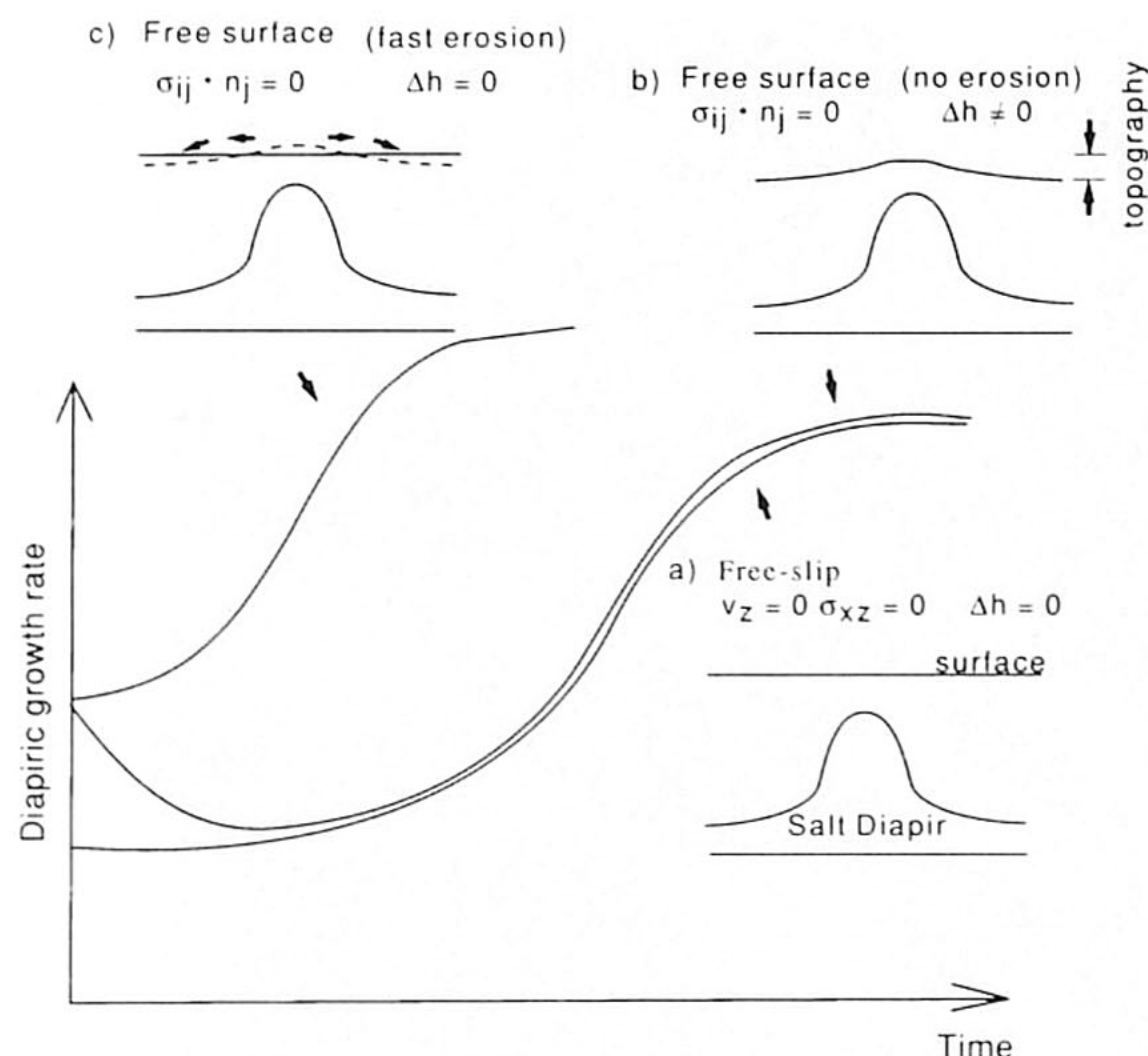


Fig. 2. (a–c) Simulated boundary conditions) and schematic scenarios of diapiric growth under different boundary conditions.

chikov, 1992) but this statement is only valid for models which do not include elasticity (J. Chery, pers. commun., 1991). Another type of boundary condition can approximate erosion of the upper surface (Fig. 2c). This erodes the surface relief created above a rising diapir by means of a diffusion equation (Kenyon and Turcotte, 1985; Syvitski et al., 1988). Material eroded from topographic highs is redeposited in lows. The volume of the problem would remain constant were no sediment to be added from an outside source (we do add sediment here). This boundary condition can easily be implemented for Eulerian meshes by keeping vertical and horizontal stresses free on the top boundary. Because the mesh does not deform, the upper surface remains flat while material can flow freely across the top boundary. Lagrangian meshes are more complicated. This is because such meshes deform as the relief on the upper surface changes. Therefore, it is necessary to change the geometry of Lagrangian meshes after each time step.

In the case of a free-slip top boundary, the velocity field has the form of a closed cell. Much the same velocity field describes the case when a free-stress boundary condition is combined with a topography. Stresses due to the topographic weight counteract the buoyancy forces and slows

consequent flow. In the case of a free-surface boundary with a flat upper surface there is no topographic weight on the imaginary mean upper surface. The upper boundary is open and no material crosses it to counteract the buoyancy forces. As a result, the velocity field has a completely different shape and the maximum velocity is 10–15 times faster than the case where the topography is not redistributed.

Typical diapirs for the three boundary conditions discussed above are shown schematically in Figure 2d. Diapirs developed beneath a free-slip top boundary and a free-surface-without-erosion top boundary are very similar; they differ only in their early stages. This is because the initially flat upper boundary rapidly returns to equilibrium after a short time. The curve representing erosion starts from the same point as the case without erosion but rises faster and thus has a shorter evolution.

The rate of evolution of diapirs displays a time spectrum with end members that depend on the erosion rate. For simplicity we will emphasize the effect of erosion on diapiric growth rate by comparing these end members.

Formulation of the problem of diapirism in compacting sediments with a redistributing topography

We present a 2-D numerical model of the viscous Rayleigh–Taylor instability in profile with an overburden that increases in area with time. This model simulates the growth of salt diapirs in sedimentary basins with compacting sediments.

The geometry and boundary conditions for the calculated models we report here are shown in Figure 3. The bottom of the box is a no-slip boundary and free-slip occurs along the left and right sides. The upper or top boundary is a free-surface with erosion in some cases, and a free-slip surface without erosion in others.

Both the salt and its overburden are assumed to have viscous rheologies. The viscosity of salt is taken as constant so that viscous forces are linearly proportional to the strain rate—as is known to be the case for salt containing more than 0.3 wt.% water (Urai et al., 1986). We follow Van

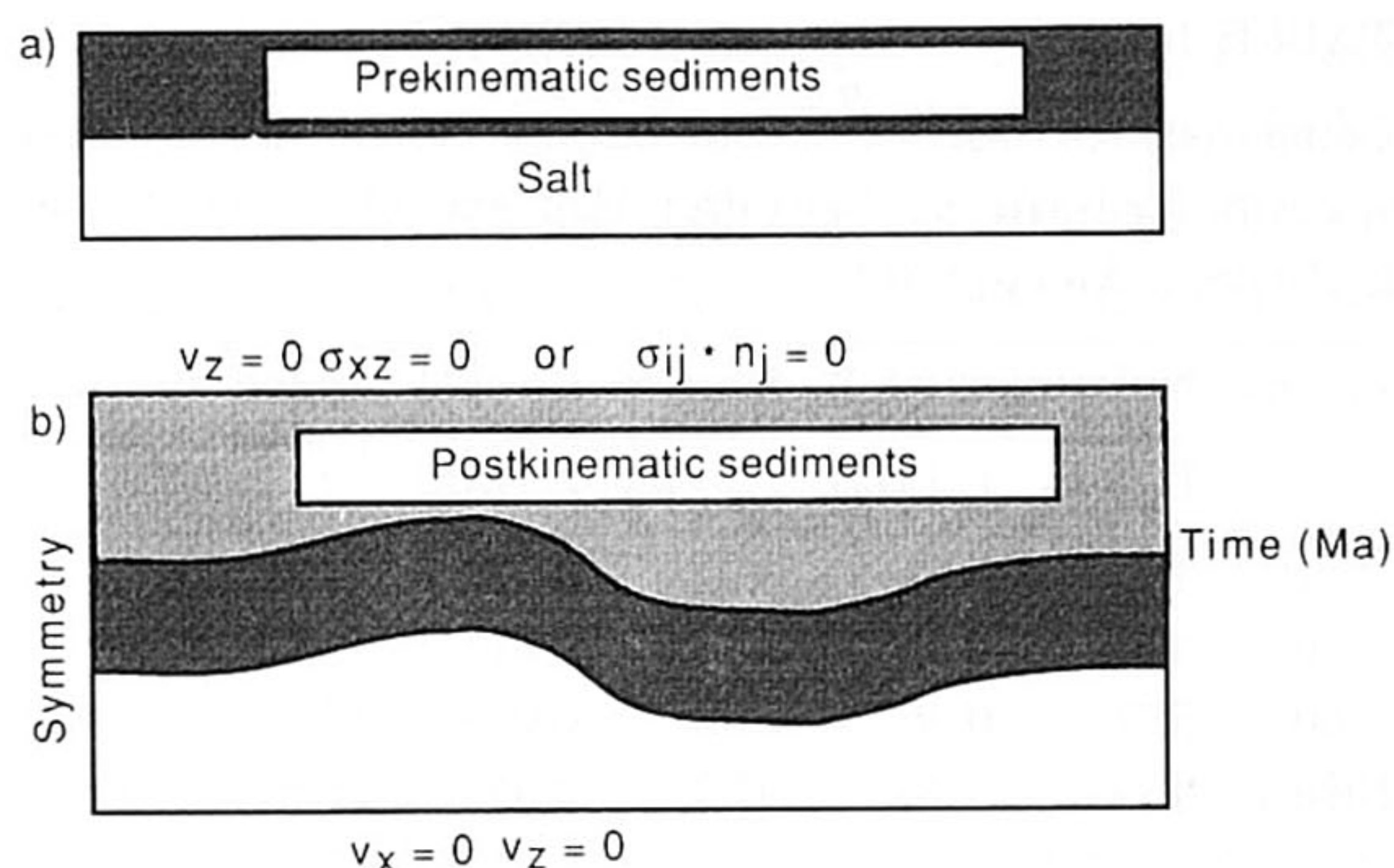


Fig. 3. Geometry of the problem at (a) time $t = 0$ (system becomes unstable) and (b) $t > 0$.

Keken et al. (1993) in assuming that non-Newtonian effects in salt are not important in determining the growth rate and geometry of salt bodies. We therefore use a viscosity equal to 10^{17} – 10^{18} Pa s which is reasonable for fine-grained salt (0.005–0.01 m) in the temperature interval 20–160°C.

We assume a viscous rather than a brittle overburden for the four reasons listed in the introduction. Very little appears to be known about the ductile rheology of sediments and, in the absence of data, we assume it to be linear and vary the value of the viscosity to simulate reasonable rise rates for salt diapirs ($\eta_{\text{sedim}} = 10^{21}$ – 10^{22} Pa s).

The Stokes equation for viscous flow is solved by a finite-element code (Poliakov and Podladchikov, 1992). For efficiency, we combine a Lagrangian method with markers that track material discontinuities and remeshes whenever the computational grid distorts unreasonably.

Salt is taken to be incompressible with a constant density ($\rho_{\text{salt}} = 2200 \text{ kg/m}^3$). By contrast, the density of the overburden increases exponentially with depth. Biot and Ode (1965) approximated Nettleton's (1934) data for the relation between density and the depth of sediments in the Gulf Coast region. This relationship (Fig. 4) can be approximated by the function:

$$\rho_{\text{sedim}} = 2.49 - 0.59 \exp(\alpha y) - \alpha y \exp(\beta y) \quad (1)$$

where $\alpha = 0.59 \times 10^{-3} \text{ m}^{-1}$, $\beta = 1.6 \times 10^{-3} \text{ m}^{-1}$, $\alpha = 5 \times 10^{-5} \text{ m}^{-1} \text{ kg/m}^2$ and $-y$ is the depth in cm.

After each time step during the simulation we determine the “depth” for each integral node and assign the corresponding density to it. This approach to relating the density of the overburden sediments to depth neglects two factors: (1) overburden volume does not change during “compaction”; and (2) sediments “decompact” during uplift (this is unrealistic if cementation occurs). However, neglecting these factors is not likely to be significant because our numerical experiments show that most overburden sinks and very little rises.

Figure 3a shows a two-layer system at time $t = 0$. The thickness of the salt (white bottom layer), h_{salt} , is 1000 m. The (dark) upper layer represents “prekinematic” sediments deposited before the salt started to move (Jackson and Talbot, 1991). The thickness of the upper layer is considered critical, so that the system is just gravitationally unstable, and taken to be equal to 1000 m. We discuss the exact meaning of this critical thickness in the next section.

A sinusoidal perturbation is imposed on the boundary between the salt and its overburden. The wavelength of this perturbation is chosen to be between 10 and 25 km which is in accord with Biot and Ode's (1965) stability analysis.

Figure 3b shows the system at an arbitrary time. The area of the region increases as the overburden thickens due to the arrival of sediments from outside the reference frame. Layers of sediments are distinguished by markers with ages shown on the right side.

Biot and Ode's theory for the initial stages of diapirism due to gravitational instability with a compacting and thickening overburden

Effect of erosion

We repeat here the basic results of Biot and Ode's (1965) analysis to justify the parameters we use in our models. These workers studied the stability of a two-layer system (similar to that in Fig. 3b) during the early stage of the growth of salt structures. They chose the following parameters for the bottom layer in their model: $\eta_2 = 10^{16}$ Pa s; $h_2 = 10^3 \text{ m}$; $\rho_2 = 2.2 \times 10^3 \text{ kg/m}^3$.

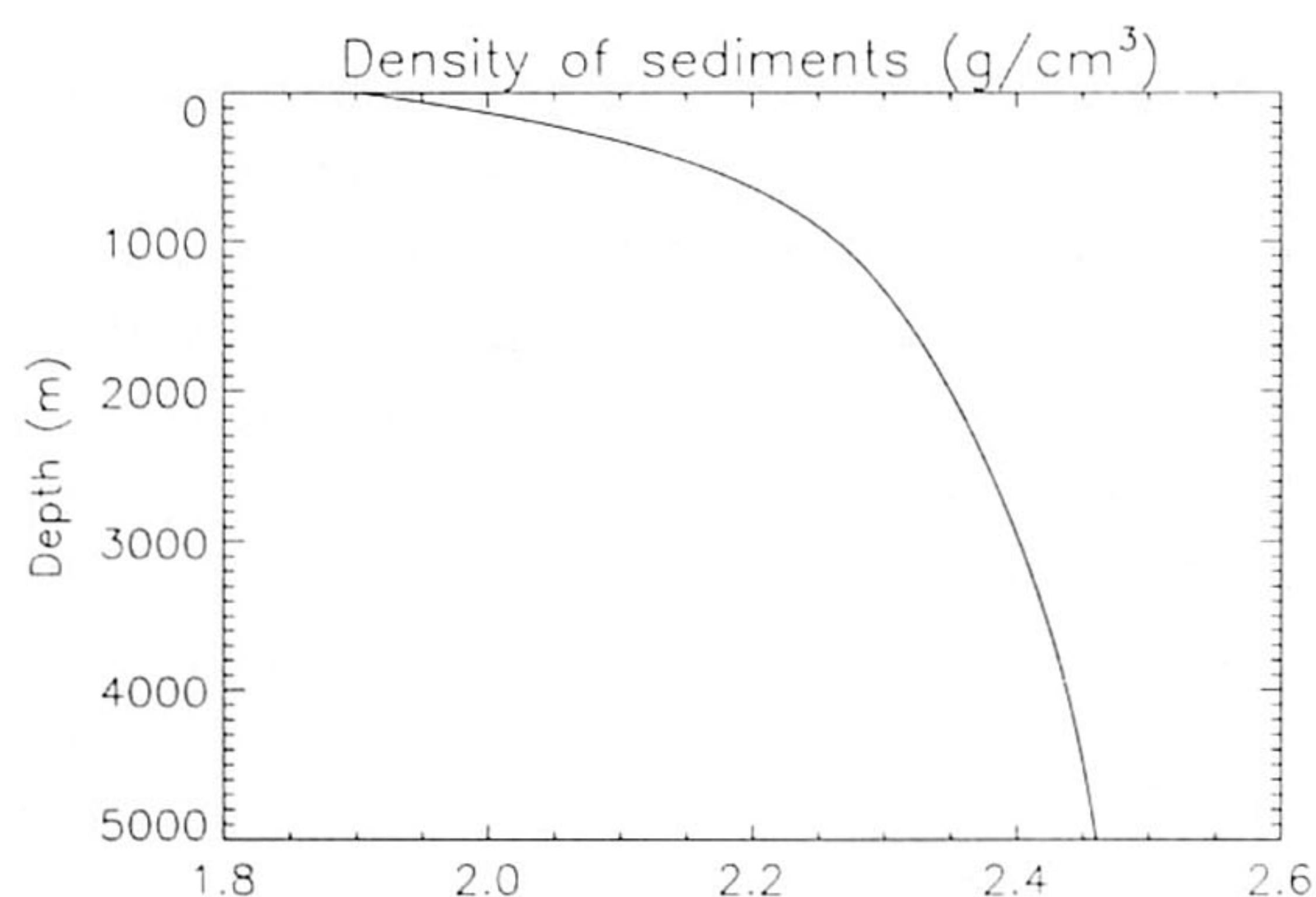


Fig. 4. Density–depth relation for Gulf Coast sediments (after Biot and Ode, 1965).

We wish to study the growth rate for different wavelengths L and identify the dominant L_d (i.e. fastest growing or characteristic) wavelength. In stability problems, the solutions (for amplitudes (U, V) , velocities (\dot{U}, \dot{V}) and stresses σ_{ij}) are proportional to the exponential factor:

$$U, V, \dot{U}, \dot{V}, \sigma_{ij} \propto \exp(pt)$$

where t is time. The growth factor p is proportional to the buoyancy forces and inversely proportional to the viscosity of the upper layer η_1 :

$$p = \frac{(\rho_1 - \rho_2)gh_2}{\eta_1\sigma}$$

where σ is a non-dimensional parameter that depends on the boundary conditions.

A “characteristic time” t_c is introduced as a measure of the growth rate of the instability. This is the time taken for the original amplitude of the perturbation to amplify one thousand times. We use this characteristic time to compare different cases. For example, expressions such as “the instability grows twice as fast” or “speeds-up” means that the t_c of this instability is two times less, or that p is two times higher than in a comparable case.

We summarize the tables from Biot and Ode (1965) in a more convenient form (Tables 1 and 2) to emphasize the effect of erosion and to choose parameters for our own models.

A comparison of diapirism *with* and *without* erosion shows that:

TABLE 1

Comparison of cases with and without erosion for different viscosity contrasts η_1/η_2 (after Biot and Ode, 1965); Case $h_1/h_2 = 1$, $\Delta\rho/\rho_1 = 0.1$

η_1/η_2	No erosion		Erosion		Speed-up ($t_c^{\text{no eros}}/t_c^{\text{eros}}$)
	L_d/h_2	t_c (Ma)	L_d/h_2	t_c (Ma)	
1	3.14	0.01	3.92	0.007	1.43
10	3.95	0.05	5.76	0.012	3.83
100	5.71	0.36	8.37	0.026	13.8
1000	8.72	3.36	12.2	0.059	56.9

— the *characteristic wavelength* is longer with erosion than without (although it is only up to 1.5 times higher for $h_1/h_2 > 1$).

— the *growth rate of the instability* depends on (a) the wavelength, (b) the viscosity contrast between the two layers and (c) the thickness of the overburden, and is higher for diapirism with erosion. It depends on (a) the wavelength, (b) the viscosity contrast between the two layers and (c) the thickness of the overburden (Table 1 and 2):

(a) For *short* wavelengths the growth rates are almost the same, but there is a considerable difference for wavelengths of the order of, or longer than, the *dominant wavelength*.

(b) Growth factors are very different for *high viscosity contrasts*. For example, at $\eta_1/\eta_2 = 10^3$ the instability with erosion grows approximately 57 times faster than without erosion. (Note, this comparison is only approximate because the dominant wavelengths differ in each case.)

(c) A thin upper layer greatly reduces the characteristic time t_c . The instability is more than 3000 times faster for $h_1/h_2 = 0.1$ but only three times faster for $h_1/h_2 = 5$.

TABLE 2

Comparison of the cases with and without erosion for different thickness ratios h_1/h_2 (after Biot and Ode (1965); Case $\eta_1/\eta_2 = 10^3$, $\Delta\rho/\rho_1 = 0.1$

h_1/h_2	No erosion		Erosion		Speed-up ($t_c^{\text{no eros}}/t_c^{\text{eros}}$)
	L_d/h_2	t_c (Ma)	L_d/h_2	t_c (Ma)	
0.1	1.6	32.9	4.0	0.009	3655.6
1	8.7	3.36	12.2	0.059	56.9
5	19.6	0.87	26.1	0.268	3.24
20	27.3	0.63	28.2	0.622	1.01

In summary, redistribution of potential surface topography above rising diapirs strongly influences the growth of salt diapirs in sedimentary basins where the thickness of the overburden approximates the thickness of the salt layer.

Instability with time-dependent thickness of compacting overburden

A compacting overburden can be represented by a system of numerous thin layers with depth-dependent densities $\rho(y)$. Each layer contributes to the force acting on the unstable interface between the salt and its overburden. Biot and Ode (1965) simplified this system to a single layer with an *effective density* ρ_e which acts with the same force as the multilayered system. The effective density depends on the compaction law, the thickness of the upper layer, and the *wavelength* of the perturbation of the interface.

Uncompacted sediments of the overburden start less dense than salt and the system is initially stable. The density of the deepest sediments reaches the density of salt as the overburden thickens to ≈ 600 m. However, this loading situation is *insufficient* to initiate the instability. *The system will only be unstable after the "effective density" of the whole overburden exceeds the density of salt.* The thickness of overburden at this moment is critical (h_{crit}) for the instability. This critical thickness depends on the wavelength of any perturbation of the interface between salt and sediments. For example, ρ_e is equal to 2200 kg/m^3 at $h_{\text{crit}} = 700$ m for a wavelength $L = 3$ km and at $h_{\text{crit}} = 900$ m for $L = 20$ km.

Another important factor is that the *dominant wavelength is not constant* and *increases* during overburden growth. Thus, there are *instantaneous* fastest growing wavelengths and the physically dominant one is expected to be that which is amplifying most at a given time. For a thin overburden ($h_1 < 2$ km), short wavelengths $L \approx 10$ km grow faster than longer wavelengths and soon reach a constant growth rate. The rate of growth for longer wavelengths $L \approx 20$ km continues to increase as the overburden thickens although the instability slows for very long wavelengths ($L > 30$ km). Different wavelengths compete in growth

rate during sedimentation. Because the growth rate is dependent on overburden thickness and, therefore, on the sedimentation rate and time, the amplification of the instability can be found by integration of $p(L, t)$ in time for different L .

Biot and Ode (1965) showed that the *dominant wavelength is shorter for slow sedimentation* than for fast sedimentation. However, they found the difference to be quite small. They also showed that the *amplification of the instability is not very selective in a broad band of wavelength* with $10 < L < 25$ km. In other words: all wavelengths in this spectrum grow at similar rates. Schmeling (1987) used numerical models to study this interaction between characteristic and non-characteristic wavelengths. He found that short initial wavelengths may be suppressed by a faster growing characteristic wavelength only if their lengths differ by several orders of magnitude and if the amplitude of the initial perturbation is small compared to its wavelength.

Choice of initial parameters for the numerical model

We can now use the results compiled in the last section to choose appropriate parameters for our numerical models. The critical thickness of the overburden should be at least 900 m for the instability to start amplifying and we take it to be 1 km. Selecting the initial wavelength for the perturbation is critical. Because of the wide spectrum of wavelengths which can amplify at similar rates, we can choose a wavelength somewhere between $10 < L < 25$. However, Schmeling's (1987) results indicate the difficulty of changing the initially triggered wavelength. We therefore suggest that shorter wavelengths ($10 < L < 15$) dominate the initial stages and that mature diapirs will inherit the same range. It is difficult to compare diapirism with and without erosion because the upper boundary conditions change as well as the dominant wavelength.

We therefore choose the following initial parameters in the model for overburden:

$\eta_1 = 10^{20} \text{ Pa s}$; $h_1^{\text{init}} = 10^3 \text{ m}$; $\rho_1 = \rho_{\text{sedim}}(y)$ (from eqn. 1).

and for salt:

$\eta_2 = 10^{17} \text{ Pa s}$; $h_2 = 10^3 \text{ m}$; $\rho_2 = 2.2 \times 10^3 \text{ kg/m}^3$.

TABLE 3

Names of the models for different sedimentation rates and boundary conditions on the upper surface

Sedimentation rate (m/Ma)	Model name	
	No erosion	Erosion
50	ner50	er50
500	ner500	er500

The horizontal length of the model is 20×10^3 m. This length contains 1.5 periods of a cosine perturbation ($L \approx 13.3$ km) with an initial amplitude $\Delta h_{\text{perturb}} = 30$ m.

Diapirism at different sedimentation rates and the influence of erosion on non-linear stages

Because salt diapirism is controlled by the thickness of the overburden, the rate of sedimentation is a very important parameter in the modeling. We explored this influence by calculations simulating slow (50 m/Ma) and fast sedimentation rates (500 m/Ma) with different boundary conditions. The models are labeled in Table 3. To compare models with and without erosion we use the same sedimentation history for each model. In all models the final thickness of the complete sedimentary package h_1^{final} is 5 km. If the diapirs are still immature when the overburden reaches this thickness, the sedimentation rate is reset to zero and the diapirs are allowed to rise.

The diffusion equation for modeling erosion and sedimentation

Geomorphologists and civil engineers have used the diffusion approach to model the long-term behavior of river systems for many years (Angevine et al., 1990). The diffusion model has also proved useful for studying the development of river delta's in fjords and glacial lakes (Sylvitski et al., 1988), and the development of foreland basins in front of advancing fold-thrust belts (Flemings and Jordan, 1989; Sinclair et al., 1991).

The governing equation is:

$$\frac{\partial h}{\partial t} = K \frac{\partial^2 h}{\partial x^2} \quad (2)$$

where h is the topographic height, t the time, K the transportation coefficient and x the horizontal distance (Kenyon and Turcotte, 1985).

This equation expresses the law of conservation of mass: the change in elevation of the topography is caused by the local divergence of sediment fluxes. The sediment flux depends on the topography. Justification of the equation depends on the transportation medium. The effect of gravity on random motions of particles in air or water (due to bioturbation, wave induced pressure variations, freezing and thawing, etc.) relates the sediment flux to the topography. Sliding processes active on delta fronts and shelf edges characteristically occur at low angles. The gravitational driving force for these slides is approximately linearly proportional to the topography. Intuitively, the number of slides (and thus the total mass transported) varies linearly with the topography (Kenyon and Turcotte, 1985). This means that the diffusion equation is particularly appropriate for gentle water-saturated slopes. The derivation of the diffusion equation is quite complicated for fluvial systems (Angevine et al., 1990) where K represents the morphology of the river system (braided, meandering, etc.), the total amount of water available, and the type of sediment transported. However, there seems to be general agreement that the diffusion model is appropriate for simulating surficial sedimentation processes in the shallow facies of sedimentation basins (deposition, erosion, resuspension, redistribution, resedimentation, etc.). We consider this sufficient justification for using diffusion to simulate surface processes during downbuilding of salt diapirs.

Diapirism with fast erosion

We will use the term "fast erosion" in the sense that material is redistributed so fast that the upper surface is always flat. No sediments leave the system and new sediments form outside the system are deposited everywhere on the top surface at the same rate. Fountains of salt extruding under the skies of Iran (Talbot and Jarvis, 1984) or the waters of gulf of Mexico (Nelson, 1991), suggest that topographic domes of salt are

not always redistributed as fast as the surrounding clastic sediments. Nonetheless we make no distinction here between salt and overburden and redistribute equally fast any relief in both materials.

Figure 5 shows the “er50” model in which erosion and sedimentation were equally slow at 50 m/Ma. Sedimentation was so slow compared to the growth of the instability that the crests of both diapirs rose above the 1 km deep level of neutral buoyancy and had very nearly surfaced by about 2 Ma. However, although the two diapirs assumed “plug-like” shapes with almost vertical contacts they did not actually reach the surface even after 10 Ma (top diagram, Fig. 5). What look like flat solution-truncated crests (Jackson and Seni, 1984) are not. After 10 Ma the maximum thickness of the overburden was only about 1.5 km thick and the weights of adjacent columns of overburden and salt were approximately equal. This meant that the buoyancy forces were insufficient for the diapirs to pierce the veneers of uncompacted overburden accumulating on them and extrude onto the surface. (The diapirs could have surfaced and extruded if the overburden had compacted faster with depth than in this model.) This system was evolving towards a ge-

ometry with minimum potential energy with salt spread in a horizontal sheet along its level of neutral buoyancy.

Figure 6 illustrates the evolution of “er500”, a model with both fast sedimentation and fast erosion. At 500 m/Ma, the sedimentation rate in this model was sufficiently high that the effective overburden was always thicker than in equivalent stages in other models. The pressure difference responsible for the buoyancy that drives diapirs upwards is proportional to the thickness of the overburden. If all other factors are kept constant, then the driving forces associated with rapid sedimentation always exceed those induced by slow sedimentation. (Note that the average density of the overburden depends on the rate of sedimentation. It is higher for faster sedimentation because then the percentage of compacted sediments is higher.)

Builtup conformable pillows in this model (Fig. 5) had already evolved to disconformable built-down diapirs that had surfaced by about 2 Ma. After each diapir reached the surface, its flat crest remained exposed throughout the remainder of the experiment. Because the exposed tops of the diapirs erode as fast as the surrounding sediments in these models, the salt bodies de-

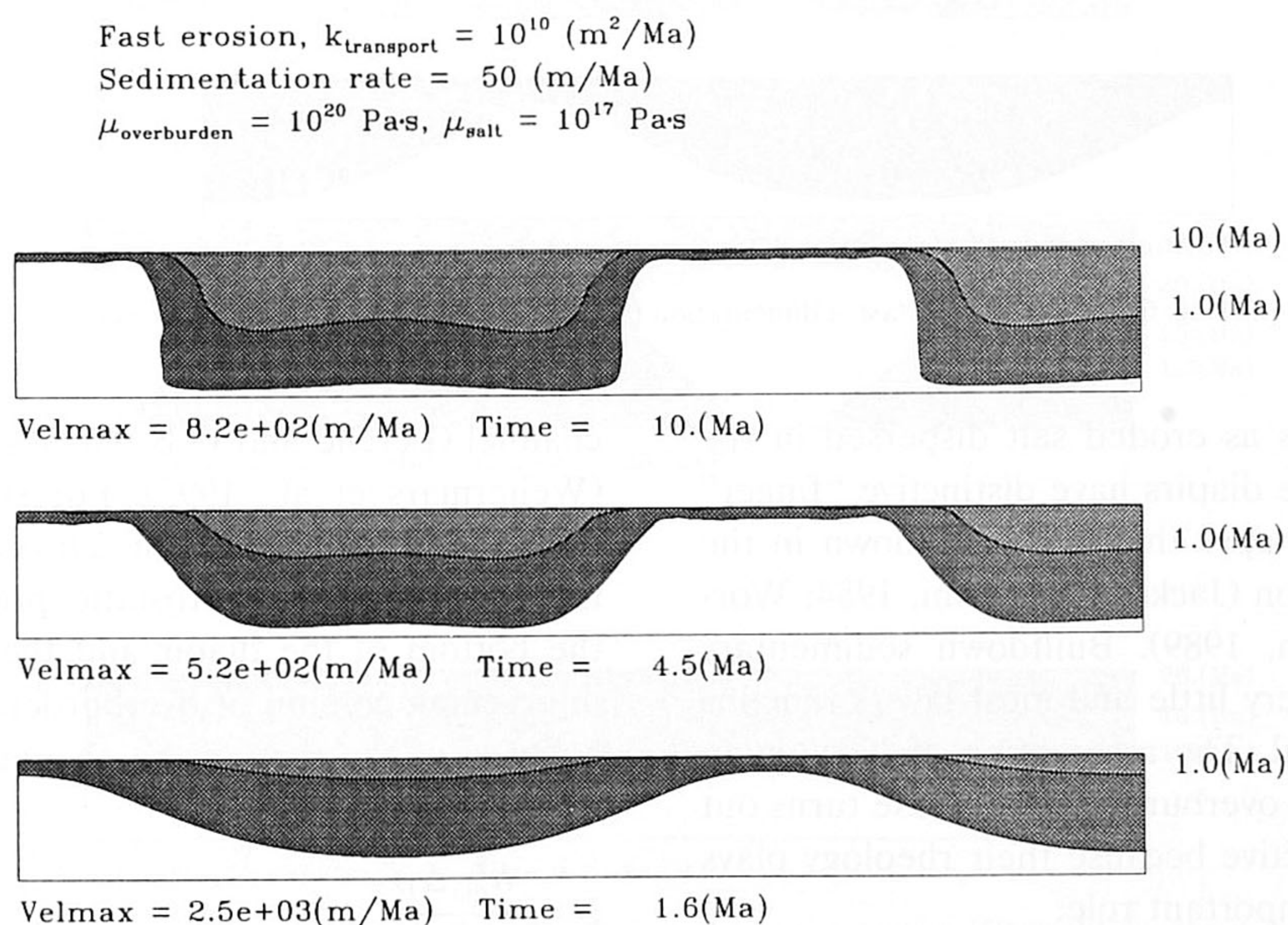


Fig. 5. Evolution of a Rayleigh–Taylor instability with thickening and compacting overburden and erosion on the upper surface. Sedimentation is slow: 50 m/Ma (model er50).

Fast erosion, $k_{\text{transport}} = 10^{10} \text{ (m}^2\text{/Ma)}$
 Sedimentation rate = 500 (m/Ma)
 $\mu_{\text{overburden}} = 10^{20} \text{ Pa}\cdot\text{s}$, $\mu_{\text{salt}} = 10^{17} \text{ Pa}\cdot\text{s}$

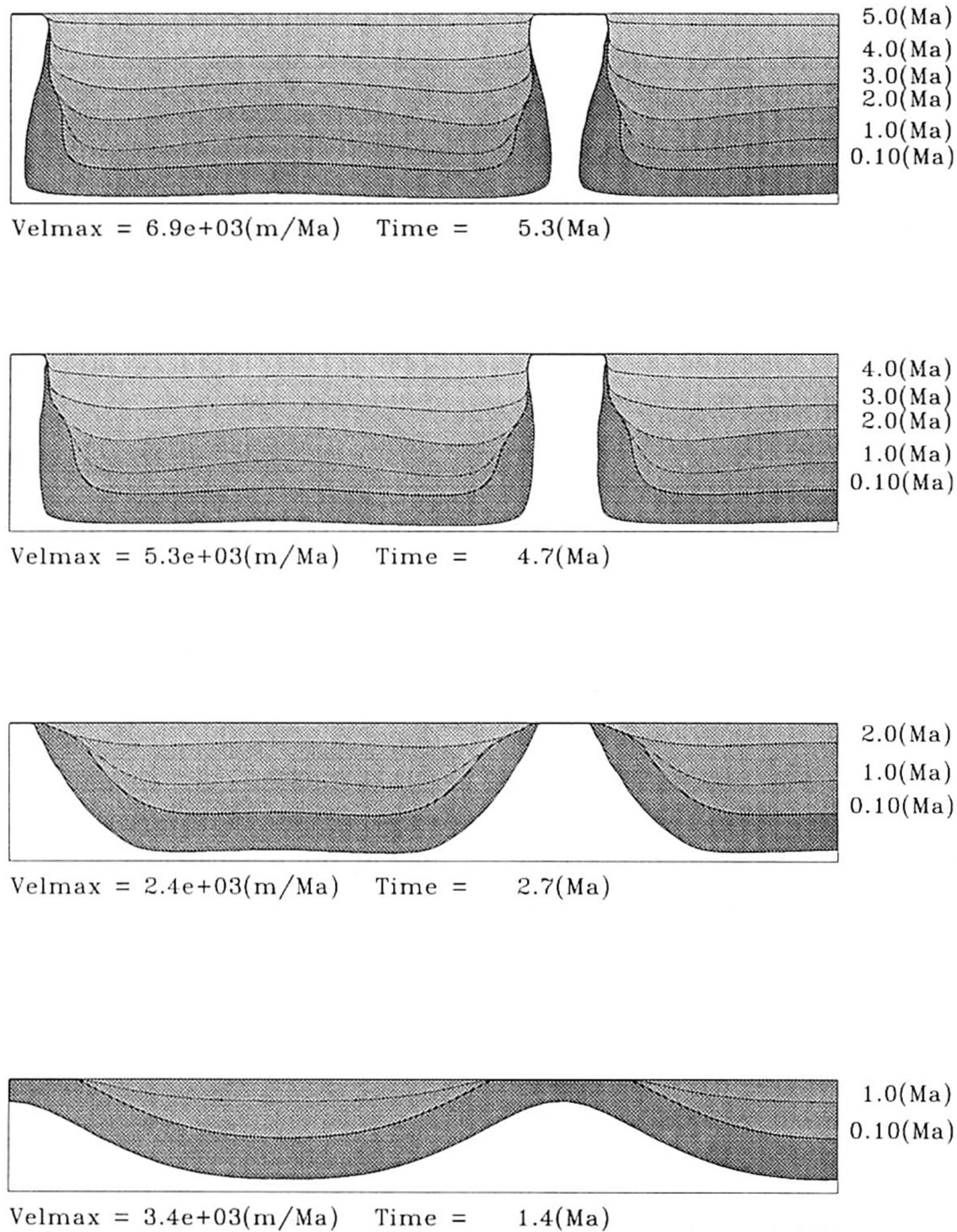


Fig. 6. Diapirism with fast sedimentation (500 m/Ma) and erosion (model er500).

creased in areas as eroded salt dispersed in the overburden. The diapirs have distinctive “finger” or “chimney” shapes that are well known in the Gulf Coast region (Jackson and Seni, 1984; Worral and Snelson, 1989). Built-down sedimentary layers deform very little and most layers remains nearly horizontal. The assumption of Newtonian rheology for the overburden in this case turns out not to be restrictive because their rheology plays a relatively unimportant role.

The extrusion of salt through an open (venting) “chimney” diapir can be approximated by

channel (Lerche and O’Brien, 1987) or pipe flow (Weijermars et al., 1993). For such approximations the pressure gradient Δp is almost equal to the difference in hydrostatic pressure between the bottom of the diapir and the bottom of the intervening column of overburden. Maximum velocity U of the flow in the channel is then equal to:

$$U = \frac{h_{\text{dia}}^2 \Delta p}{12 \eta_2 \Delta l}$$

where h_{dia}^2 , η_2 , and Δl are the thickness, viscosity

and vertical length of the open diapiric channel. Increasing the thickness of the overburden does not influence the extrusion rate because the pressure gradient $\Delta p/\Delta l$ remains constant. Nevertheless, the vertical extrusion velocity decreases because the diapir narrows as it elongates and loses area by extrusion and erosion. The extrusion rate decreased below the sedimentation rate in the late stages of Figure 6 but the diapirs continued to extrude because they were still driven by strong buoyancy forces.

Diapirism without erosion

Figure 7 illustrates the evolution of diapirs built down by slow sedimentation without any redistribution of surficial overburden ("ner50" model). Pillows mature to diapirs with bulbs that rapidly spread allochthonous sheets horizontally along their current level of neutral buoyancy. Complications then develop. The allochthonous sheets pinch off from their autochthonous source layer along the bottom boundary. Meanwhile, the

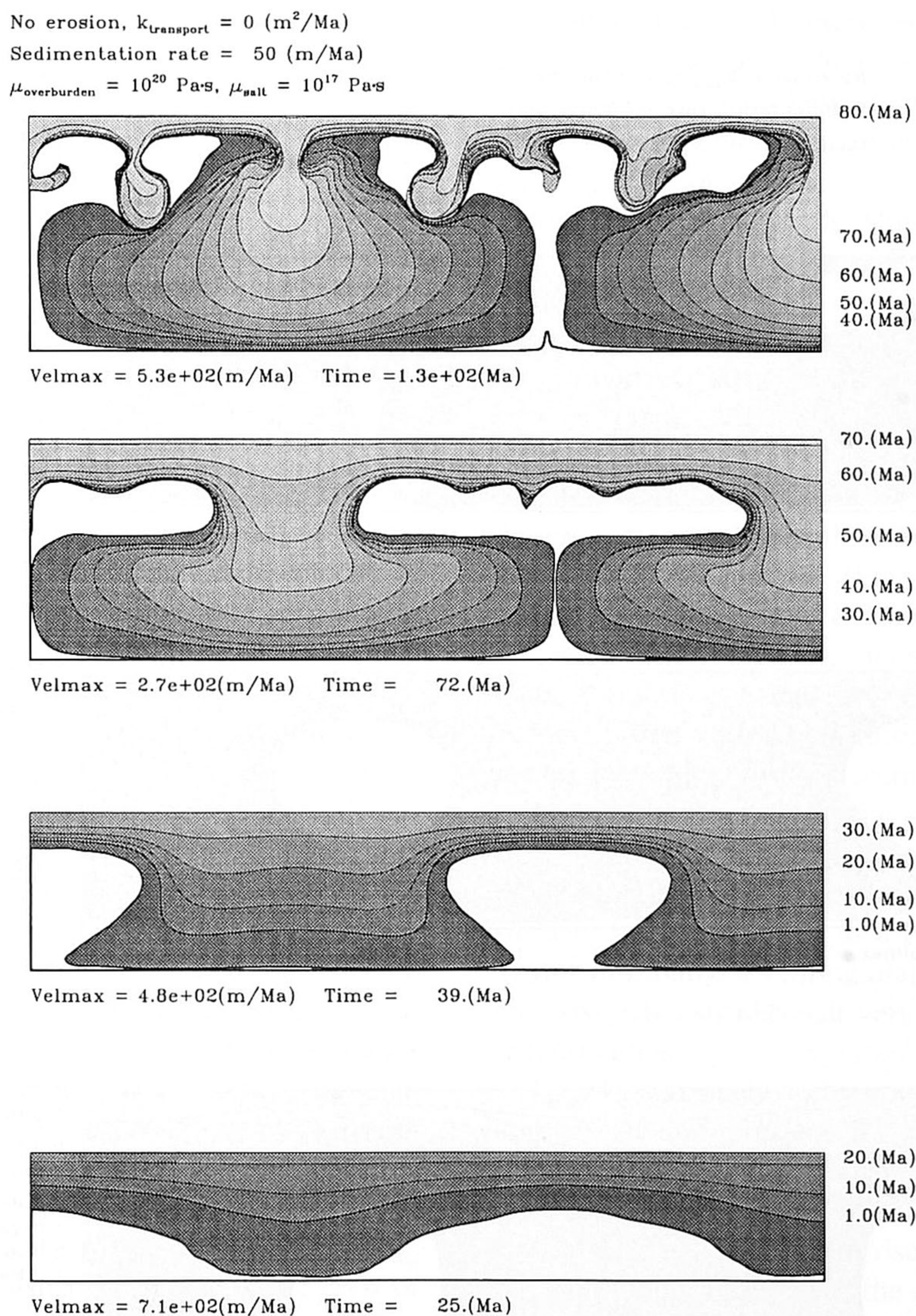


Fig. 7. The development of multiple generations of diapirs during slow sedimentation (50 m/Ma) without erosion (model ner50). Natural examples of salt diapirs like this are likely in the Nordkapp basin (Talbot et al., in press) and asymmetric versions are likely in the Gulf of Mexico (Koyi, 1991).

level of neutral buoyancy continues to rise as sedimentation continues to thicken the overburden. Eventually, overburden sedimented above the rapidly spread salt sheet compacts to an average density greater than salt. The sheet then becomes buoyant and unstable in its own right and diapirism reactivates to feed a second generation of diapirs (third diagram from bottom, Fig. 7). Because the geometry of the second instability is inevitably different from the starting configuration of the first instability, the fastest growing

wavelength of the second generation diapirs are much shorter than the first (Koyi, 1991; Talbot et al., in press). Though much smaller, the second generation diapirs eventually spread along their own levels of neutral buoyancy.

Model ner500 (Fig. 8) simulates the classical case of diapiric upbuilding. In the absence of erosion, and with sedimentation so much faster than the growth of the RT instabilities, essentially all the overburden was in place before the diapirs developed. Pillows matured into upbuilding di-

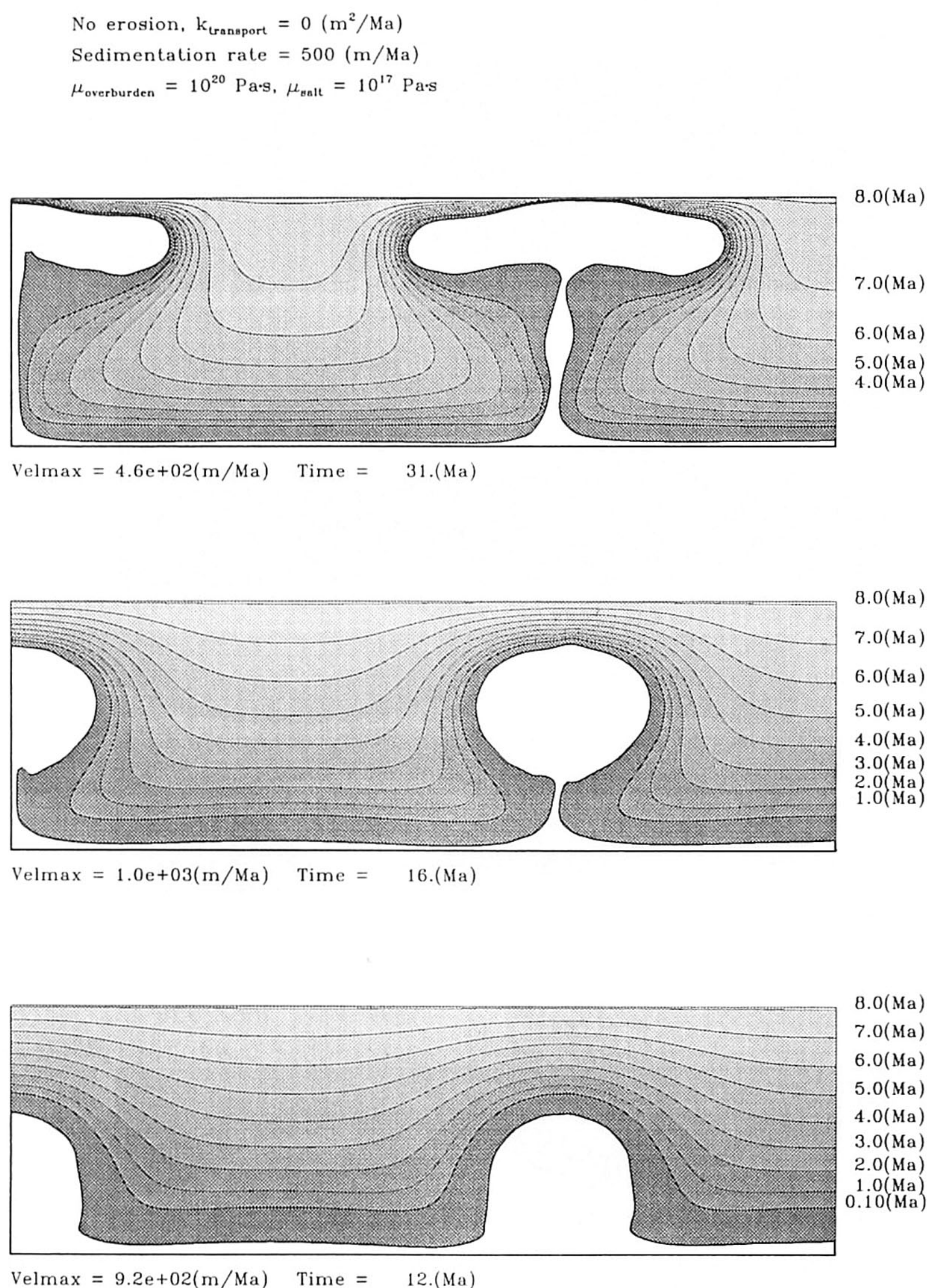


Fig. 8. Diapirs built up by rapid sedimentation (500 m/Ma) and no erosion (model ner500).

apirs with “balloon on a string” geometries. Sedimentation did not slow the rise of these diapirs because their spherical bulbs have optimal shapes for maximum buoyancy. Indeed, dynamic buoyancy forces temporarily drive these bulbs above their level of neutral buoyancy and they later have to spread downwards to reach geometries with least potential energy. In both the cases we modeled without erosion, sedimentary layers deformed continuously by viscous flow and remained smoothly conformable with the shape of the diapirs.

Scaling and generalization

We have illustrated models for diapirism at four different rates of sedimentation and erosion with all others parameters kept constant. We now explore the consequences of other parameters.

The models have the following non-dimensional parameters:

$$\frac{h_1^{\text{init}}}{h_2}, \frac{h_1^{\text{final}}}{h_2}, \frac{\Delta h_{\text{pertub}}}{h_2}, \frac{V_{\text{sed}} \eta_2}{\Delta \rho g h_2^2} = \frac{V_{\text{sed}}}{V_{\text{dia}}}$$

where K is the sediment transportation coefficient, V_{dia} , V_{sed} are the characteristic velocity of diapiric growth and aggradation rate respectively and $\Delta \rho$ is the difference between the average densities of overburden and salt.

We performed a number of runs to find which of these parameters influence diapiric evolution most strongly. The previous section showed that the ratio of the rate of erosion to the diapir rise velocity (i.e. $K/(V_{\text{dia}} h_2)$) is the most crucial parameter for controlling the type of diapirism. For example when $K/(V_{\text{dia}} h_2) = 0$ and there is no erosion (Fig. 8), the diapirs have classical “balloon-on-string” shapes. Increasing this parameter results in more “finger”-like diapirs that can eventually extrude [$K/(V_{\text{dia}} h_2) \rightarrow \infty$, fast erosion, Fig. 6].

Another important parameter is $V_{\text{sed}}/V_{\text{dia}}$ which is proportional to $V_{\text{sed}} \eta_1$. At low $V_{\text{sed}}/V_{\text{dia}}$ the sedimentation rate is so slow that the crest of the rising diapir can keep pace with sediment accumulation at the upper surface (Figs. 5, 7). These cases would more obviously be classical

downbuilding if we related velocities to the top surface (near sea level) rather than the bottom boundary. Diapirs assume “plug” shapes if the potential surface bulge is eroded as fast as it forms (Fig. 5). When there is no surface erosion, the diapir spreads an allochthonous sheet (Fig. 7). Even the second generation of diapirs cannot reach the surface despite their high characteristic velocities. At higher values of $V_{\text{sed}}/V_{\text{dia}}$ the upper surface accumulates faster than the instability can rise during its slow initial stages. As a result, the effective overburden thickness always exceeds equivalent stages with lower sedimentation rates. Greater overburden thickness means higher buoyancy forces and diapirs that rise faster. Thus, the *buoyancy force increases with increasing $V_{\text{sed}}/V_{\text{dia}} \propto V_{\text{sed}} \eta_1$* .

Our calculations clearly demonstrate the influence of $V_{\text{sed}}/V_{\text{dia}} \propto V_{\text{sed}} \eta_1$. Fast sedimentation without erosion resulted in the overburden having already reached our limiting thickness of 5 km before buoyant structures were established (bottom diagram, Fig. 8), developed “bulbous” shapes, and rapidly built up to the surface. Slow sedimentation without erosion resulted in taller diapirs with completely different shapes and very complicated rise histories (Fig. 7).

Increasing the rate of erosion and $V_{\text{sed}}/V_{\text{dia}}$ at the same time completely changes the diapir dynamics. Buoyancy forces increase because of fast sedimentation and a high initial growth rate induced by early erosion (section theory). As a result, the diapir reaches the surface, vents and then remains exposed. The mechanism of salt flow changes as soon as a diapir vents to the surface. Instead of rising as a buoyant Rayleigh–Taylor instability, a venting diapir no longer rises but passively extrudes salt very rapidly by differential loading.

$V_{\text{sed}}/V_{\text{dia}}$ strongly influences the style of diapirism. At low values of $V_{\text{sed}}/V_{\text{dia}}$ diapirs reach their level of neutral buoyancy relatively soon and continue to spread along that level. At higher values $V_{\text{sed}}/V_{\text{dia}}$ diapirs can rise above their level of neutral buoyancy, or, in the case with erosion, extrude onto the surface.

Calculations for different viscosity contrasts found quite similar results and that there are only

minor differences in diapir shapes in the range of $\eta_1/\eta_2 = 10^2$ – 10^5 Pa s if $K/(V_{\text{dia}}h_2)$ and $V_{\text{sed}}/V_{\text{dia}}$ are kept fixed. This implies that the non-dimensional parameter $V_{\text{sed}}/V_{\text{dia}}$ is convenient for analysing some cases that are not shown here. Thus, the results of run “er500” can be applied to cases with other viscosity contrasts and sedimentation rates. For example, if the viscosity of the overburden η_1 is increased one order of magnitude (to 10^{21} Pa s) and the sedimentation rate is reduced one order (to 50 m/Ma), then $V_{\text{sed}}/V_{\text{dia}}$ will remain the same as in “er500”. Because changing the viscosity contrast has relatively little effect, calculations with these new parameters would approximately repeat the results of “er500” but on a time scale ten times longer.

Comparison between modeling results and geological observations

This section compares our models with published geological interpretations of salt bodies and their surrounding sedimentary layers based on seismic profiles and drilling. We also speculate

about the evolution histories of some common geometries of natural diapirs.

Figure 9 compares a seismic profile from the Gulf of Mexico with the results of our calculations for diapirism with a high viscosity contrast, fast erosion, slow sedimentation (50 m/Ma) and a density profile in which sediments compact faster with depth than in eqn.(1). Nelson (1991) interpreted “steeply dipping beds on the left flank” to indicate that salt (Fig. 9) pierced actively before “more gently dipping beds and a small area of uplift” accompanied passive extrusion. Our numerical results show a very similar history with a “finger”-like diapir extruding passively after it surfaced by active piercement. Our numerical experiment emulates the well-known “turtleback” structure and a rim syncline that narrowed dramatically as the diapir began to vent and extrude deep salt rapidly and uniformly by channel flow.

The numerical results of model “er500” approximate the shallow levels of the Grand Saline Dome and its overburden in Texas (Fig. 10). This similarity suggests that, at least temporarily, clas-

Infinitely fast erosion, $k_{\text{transport}} = \infty$
Sedimentation rate = 50(m/Ma)
 $\mu_{\text{overburden}} = 10^{22}$ Pa.s, $\mu_{\text{salt}} = 10^{16}$ Pa.s

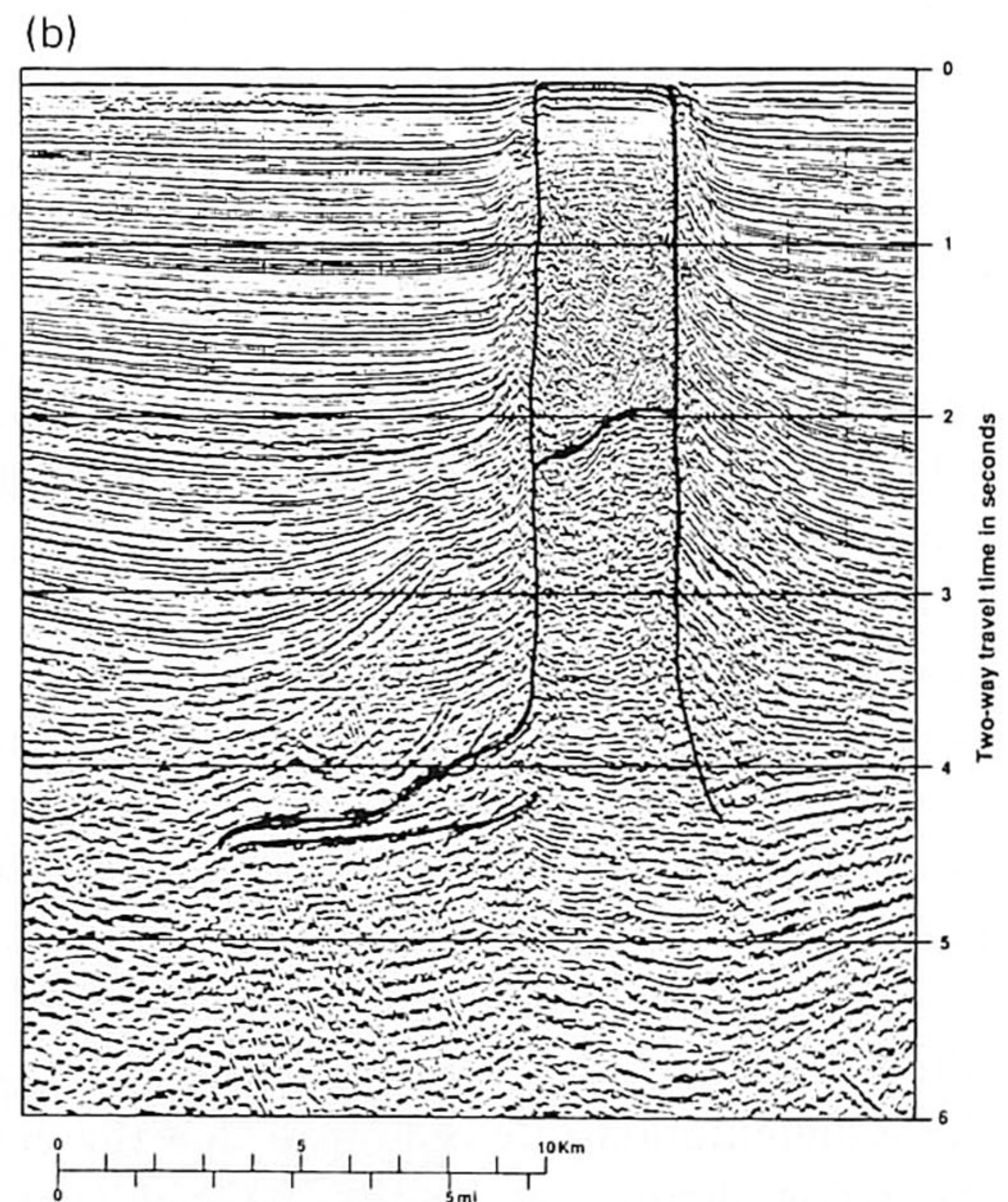
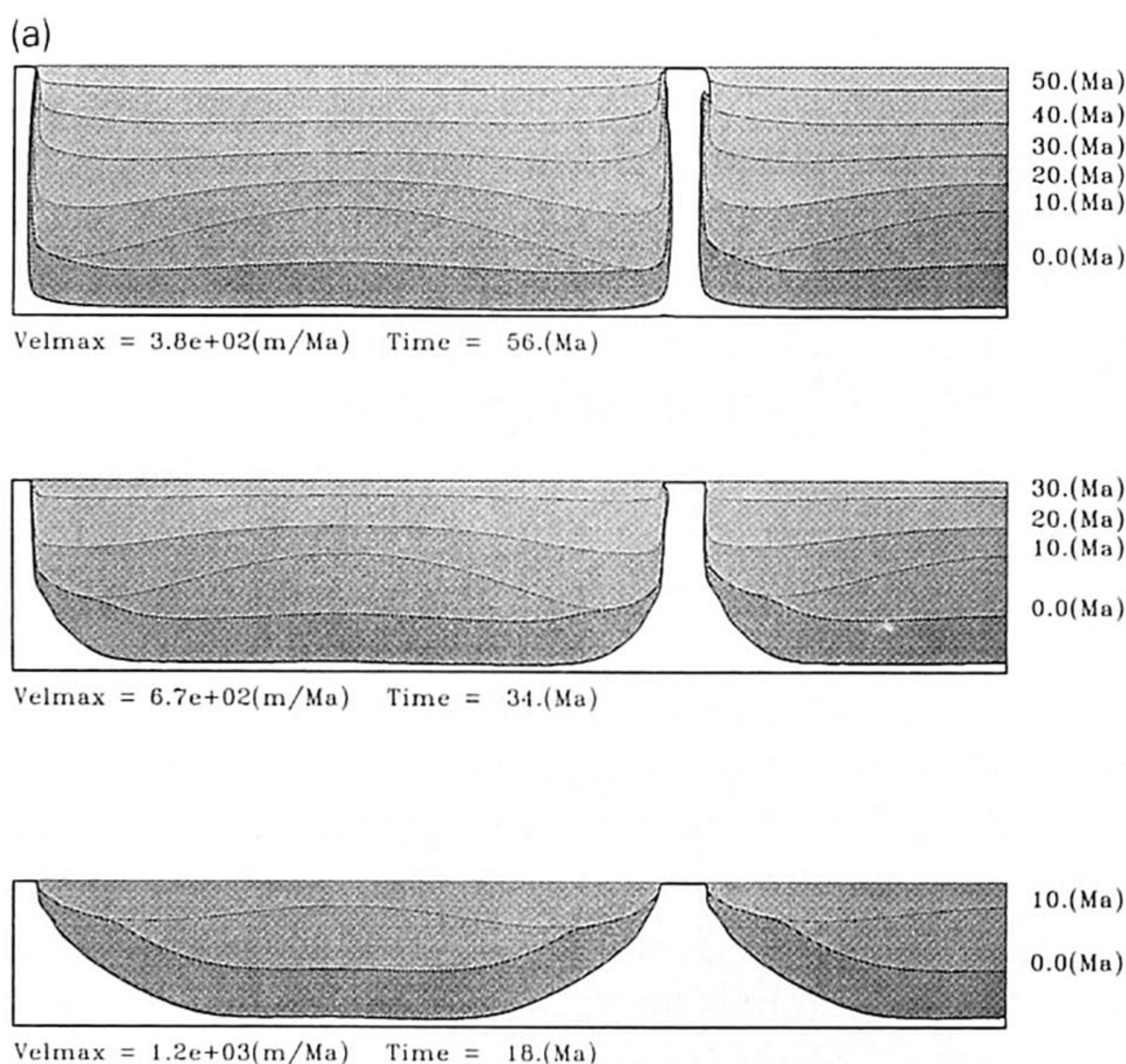
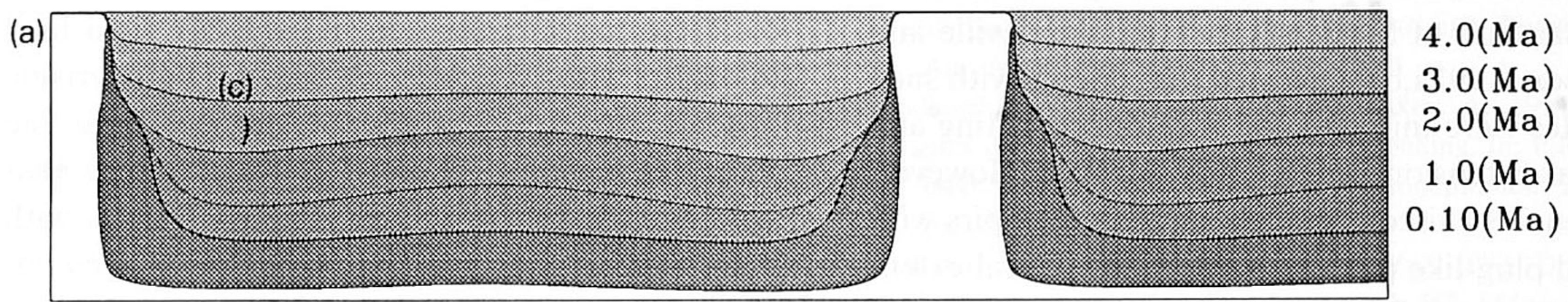


Fig. 9. Comparison of (a) a model of diapirism with a high viscosity contrast and fast erosion with (b) a seismic profile from the Gulf of Mexico region (after Nelson, 1991).

Fast erosion, $k_{\text{transport}} = 10^{10} \text{ (m}^2/\text{Ma)}$

Sedimentation rate = 500 (m/Ma)

$\mu_{\text{overburden}} = 10^{20} \text{ Pa}\cdot\text{s}$, $\mu_{\text{salt}} = 10^{17} \text{ Pa}\cdot\text{s}$



Velmax = $5.3 \times 10^3 \text{ (m/Ma)}$ Time = 4.7(Ma)

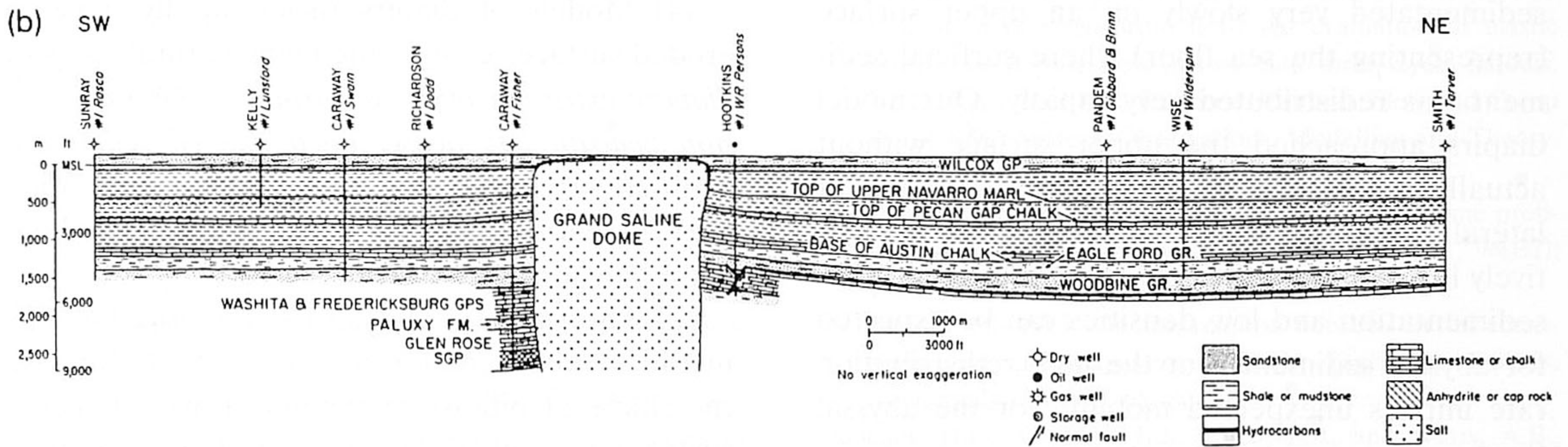


Fig. 10. Comparison of (a) model “er500” (fast downbuilding with fast surface redistribution) with (b) the Grand Saline Dome in East Texas (after Jackson and Seni, 1984).

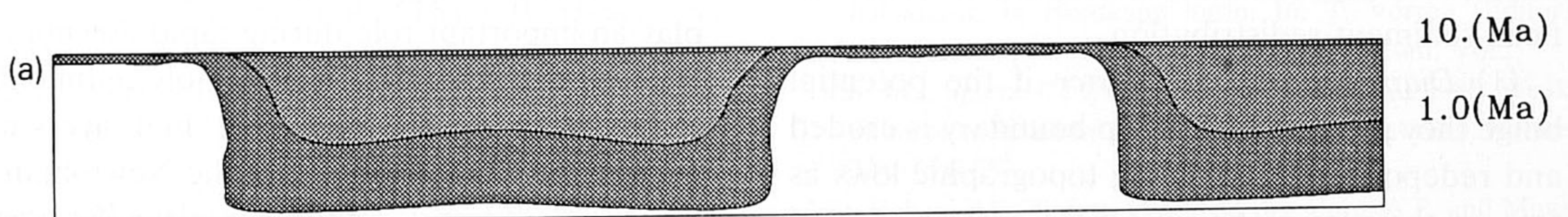
tic sediments surrounding the Grand Saline Dome was built down rapidly on a mobile surface where surficial redistribution kept topography to a mini-

mum. Passive piercement in Figure 10 began longer after initiation than it began in Figure 9 so that “er500” diapirs have thicker stems, less pro-

Fast erosion, $k_{\text{transport}} = 10^{10} \text{ (m}^2/\text{Ma)}$

Sedimentation rate = 50 (m/Ma)

$\mu_{\text{overburden}} = 10^{20} \text{ Pa}\cdot\text{s}$, $\mu_{\text{salt}} = 10^{17} \text{ Pa}\cdot\text{s}$



Velmax = $8.0 \times 10^2 \text{ (m/Ma)}$ Time = 10.(Ma)



Fig. 11. Comparison of (a) model “er50” with slow sedimentation and fast erosion with (b) a seismic profile of the Segsbee Knolls diapirs of Challenger Salt, abyssal Gulf of Mexico (after Vendeville and Jackson, 1992a).

nounced “turtle structures” and peripheral sinks with a more bimodal history.

The plug shape of our model diapirs that rose during slow sedimentation (Fig. 11) is gratifyingly similar to a seismic profile of diapirs under the abyssal Gulf of Mexico (Fig. 11b). Vendeville and Jackson (1992a,b) suggested that diapirs with such profiles were initiated and rose during rifting and lateral extension in the Early Jurassic. However, our entirely viscous models simulated diapirs with broad plug-like profiles without any lateral extension (Fig. 11a). The diapir in our numerical model was plug-like because a low-density overburden sedimentated very slowly on an upper surface (representing the sea floor) where surficial sediment was redistributed very rapidly. Our model diapirs approached the upper surface without actually reaching it or venting, not because of lateral extension, but because of the comparatively low average density of the overburden. Slow sedimentation and low densities can be expected for abyssal sediments but the high redistribution rate implies unexpected mobility for the abyssal floor.

Comparative analyses like those sketched above open new avenues for interpreting the geometries of diapirs and the surrounding layering in terms of their environmental histories.

Conclusions

In order to show the influence of erosion and redeposition of clastic sediments on the development of salt diapirs we have emphasized the main differences between models with and without surficial sediment redistribution.

(1) *Diapirs grow much faster* if the potential bulge they produce on the top boundary is eroded and redeposited in adjoining topographic lows as fast as they form. During their early stages of linear growth, diapirs rise 50 times faster with erosion than without (see section theory). More developed diapirs rise 10–20 times faster with surficial sediment redistribution than without.

(2) *The morphology of the velocity field* is completely different with and without erosion and redeposition. With no surficial redistribution, the velocity field has a closed “cell-like” structure

and varies smoothly through both overburden and diapir. With redistribution, the velocity field segregates into narrow diapiric channels with high vertical velocities separated by wide zones of slowly subsiding overburden.

(3) Strong variations in the velocity field lead to diapirs with very *different shapes*. Diapirs rising beneath rapidly redistributed surfaces have the shapes of narrow “columns” or wide “plugs” that are common in natural salt diapirs. Diapirs with “mushroom” and “balloon-on-string” shapes imply the absence of surface erosion, but are rare in nature (or rarely detected).

(4) Models of diapirs rising rapidly beneath eroded surfaces explain the many natural cases of *diapiric extrusion over the surface or lateral intrusion beneath less dense, uncompacted sediments*. Without surface erosion *diapirs spread along their level of neutral buoyancy* which is typically about 1 km beneath the surface.

(5) The velocity field also shapes the layering in the overburden. Layers smoothly conform to the shape of pillows or diapirs growing beneath surfaces not subject to erosion. For cases with fast sedimentation and fast redistribution of topography, the velocity field in the overburden is nearly uniformly downwards. Uniform subsidence of the overburden under a rapidly redistributed topography builds flat shallow layers over deep turtlebacks.

(6) The parameter $V_{\text{sed}}/V_{\text{dia}}$ controls diapir relief. Increasing this parameter drives the crest of diapirs further above its level of neutral buoyancy.

(7) The rheology of the overburden does not play an important role during rapid downbuilding because the deformation of rapidly sedimentated sedimentary layers is negligible. Flat layers in the overburden demonstrate that the Newtonian rheology we used as a simplification for the complex rheologies of natural overburdens is admissible in cases of rapid downbuilding.

Acknowledgements

Vladimir Laykhovsky is thanked for helpful discussion and hints during this work. A. Poliakov is very grateful for support provided him during

his visit to Minnesota. We are grateful to the Minnesota Supercomputer Institute, Uppsala University and the Vrije Universiteit for excellent computer facilities. Constructive reviews of earlier versions of this report by Dr. J.M. Larroque and Prof. G. Ranalli are very much appreciated. This work is a part of a project of Russian-Swedish collaborative research sponsored by the Swedish Royal Academy of Sciences who supported Y. Podladchikov during his year-long stay at Uppsala University. R. van Balen and B. Daudre are supported by the Dutch Ministry of Economic Affairs.

References

- Angevine, C.L., Heller, P. and Paola, C., 1990. Quantitative sedimentary basin evolution. AAPG, Continuing Educ. Course Note Ser. 32.
- Biot, M.A. and Ode, H., 1965. Theory of gravity instability with variable overburden and compaction. *Geophysics*, 30(2): 215–227.
- Daudre, B., Poliakov, A., Van Balen, R., Cloetingh, S. and Stephenson, R., 1992. Salt diapirism and mechanics of sedimentary basins. *Ann. Geophys., Suppl.*, 10: C91.
- Flemings, P.B. and Jordan, T., 1989. A synthetic stratigraphic model of foreland basin development. *J. Geophys. Res.*, 94: 3851–3866.
- Jackson, M.P.A. and Seni, S.J., 1984. Atlas of salt domes in the East Texas Basin. *Tex. Univ. Bur. Econ. Geol., Rep. Invest.* 140.
- Jackson, M.P.A. and Talbot, C.J., 1991. A glossary of salt tectonics. *Tex. Univ. Bur. Econ. Geol., Geol. Circ.* 91-4.
- Jackson, M.P.A., Talbot C.J. and Cornelius, R.R., 1988. Centrifuge modelling of the effect of aggradation and progradation on syndepositional salt structures. *Tex. Univ. Bur. Econ. Geol., Rep. Invest.* 173.
- Jackson, M.P.A., Cornelius, R.R., Craig, C.H., Gansser, A., Stoklin, J. and Talbot, C.J., 1990. Salt diapirs of the Great Kavir, Central Iran. *Geol. Soc. Am., Mem.* 177, 139 pp.
- Jenyon, M.K., 1986. *Salt Tectonics*. Elsevier, Amsterdam, 191 pp.
- Kenyon, P.M. and Turcotte, D.L., 1985. Morphology of a delta prograding by bulk sediment transport. *Geol. Soc. Am. Bull.*, 96: 1457–1465.
- Koyi, H., 1991. Mushroom diapirs penetrating into high viscous overburdens. *Geology*, 19: 1229–1232.
- Lerche, I. and O'Brien, J.J., 1987. Modelling of buoyant salt diapirism. In: I. Lerche and J.J. O'Brien (Editors), *Dynamical Geology of salt and Related Structures*. Academic Press, New York, NY, pp. 129–162.
- Martin, R.G., 1980. Distribution of salt structures in the Gulf of Mexico: Map and descriptive text. U.S. Geol. Surv., Map MF-1213.
- Nelson, T.H., 1991. Salt tectonics and listric normal faulting. In: A. Salvador (Editor), *The Gulf of Mexico Basin. (The Geology of North America, Vol. J.)*. Geological Society of America, Boulder, CO, pp. 73–89.
- Nettleton, L.L., 1934. Fluid mechanics of salt domes. *Bull. Am. Assoc. Petr. Geol.* 18: 1175–1204.
- Podladchikov, Yu., Talbot, C. and Poliakov, A., 1993. Complex diapiric structures: Forward modelling. In: P.R. Cobbold (Editor), *Salt Tectonics. Tectonophysics*, 228 (in press).
- Poliakov, A.N. and Podladchikov, Yu.Yu., 1992. Diapirism and topography. *Geophys. J. Int.*, 109: 553–564.
- Poliakov, A.N.B., Cundall, P., Podladchikov, Y. and Lyakhovsky, V., 1993. An explicit inertial method for the simulation of viscoelastic flow: An evaluation of elastic effects on diapiric flow in two- and three-layers models. In: D. Stone and K.E. Runcorn (Editors), *Flow and Creep in the Solar System: Observations, Modelling and Theory*. Kluwer, Dordrecht, pp: 175–195.
- Romer, M. and Neugebauer, H.J., 1991. The salt dome problem: A multilayered approach. *J. Geophys. Res.*, 96(B2): 2389–2396.
- Schmeling, H., 1987. On the relation between initial conditions and late stages of Rayleigh–Taylor instabilities. *Tectonophysics*, 133: 65–80.
- Sinclair, H.D., Coakley, B.J., Allen, P.A. and Watts, A.B., 1991. Simulation of foreland basin stratigraphy using a diffusion model for mountain belt uplift and erosion: an example from the Central Alps, Switzerland. *Tectonics*, 10(3): 599–620.
- Syvitski, J.P.M., Smith, J.N., Calabrese, E.A. and Boudreau, B.P., 1988. Basin sedimentation and the growth of prograding deltas. *J. Geophys. Res.*, 93: 6895–6908.
- Talbot, C.J., 1992. Centrifuge models of Gulf of Mexico profiles. *Mar. Pet. Geol.*, 9: 412–432.
- Talbot, C.J. and Jarvis, R.J., 1984. Age, budget and dynamics of an active salt extrusion salt in Iran. *J. Struct. Geol.*, 6: 521–524.
- Talbot, C.J., Koyi, H. and Clark, J., in press. Multiphase halokinesis in Nordkapp basin. In: T. Vorren (Editor), *Arctic Geology and Petroleum Potential. Conf. Vol.*
- Urai, J.L., Spiers, C., Zwart, C.J. and Lister, G., 1986. Weakening of rock salt by water during long term creep. *Nature*, 324: 554–557.
- Van Keken, P.E., Spiers, C.J., Van den Berg, A.P. and Muzzi, E.J., 1993. The effective viscosity of rocksalt: Implementation of steady state creep laws in numerical models of salt diapirism. *Tectonophysics*, 225: 457–476.
- Vendeville, B.C. and Jackson, M.P.A., 1992a. The rise of diapirs during thin-skinned extension. *Mar. Pet. Geol.*, 9: 354–371.
- Vendeville, B.C. and Jackson, M.P.A., 1992b. The fall of diapirs during thin-skinned extension. *Mar. Pet. Geol.*, 9: 331–353.

- Weijermars, R., Jackson, M.P.A. and Vendeville, B., 1993. Rheological and tectonics modelling of salt provinces. *Tectonophysics*, 217: 143–174.
- Woidt, W.D., 1978. Finite element calculation applied to salt dome analysis. *Tectonophysics*, 50: 369–386.
- Worral, D.M. and Snelson, S., 1989. Evolution of the northern Gulf of Mexico, with emphasis on Cenozoic growth faulting and the role of salt. In: A.W. Bally and A.R. Palmer (Editors), *Geology of North America—An overview*. (The Geology of North America, Vol. A). Geological Society of America, Boulder, CO, pp. 97–138.
- Zaleski, S. and Julien, Ph., 1992. Numerical simulation of Rayleigh–Taylor instability for single and multiple salt diapirs. *Tectonophysics*, 206: 55–69.